EARTH SURFACE PROCESSES AND LANDFORMS, VOL. 22, 59–77 (1997)

MODELLING FLOOD HYDRAULICS AND OVERBANK DEPOSITION ON RIVER FLOODPLAINS

A. P. NICHOLAS*

School of Geography, University of Leeds, Leeds, West Yorkshire, LS2 9JT, U.K.

D. E. WALLING

Department of Geography, University of Exeter, Exeter, Devon, EX4 4RJ, U.K.

Received 3 November 1994
Accepted 8 September 1995

ABSTRACT

This paper outlines a numerical model for the prediction of floodplain inundation sequences, overbank deposition rates and deposit grain size distributions. The model has two main components: first, a simplified hydraulic scheme which predicts floodwater flow depths and velocities, and second, a sediment transport element which employs a mass balance relation describing suspended sediment dispersion by convective and diffusive processes and sediment deposition as a function of particle settling rates. These relationships are solved numerically on a finite difference grid that accurately replicates the complex topographic features typical of natural river floodplains. The model is applied to a 600 m reach of the River Culm, Devon, U.K. using data derived from a range of field and laboratory techniques. Continuous records of river stage and suspended sediment concentration provide the model's upstream boundary input requirements. These are supplemented by measurements of the *in situ* settling characteristics of the suspended sediment load. The model's sediment transport component is calibrated with the aid of a dataset of measured overbank deposition amounts derived from flood events over a 16 month period. The model is shown to predict complicated floodwater inundation sequences and patterns of suspended sediment dispersion and deposition, which are largely a product of the complex topography of the floodplain. These results compare favourably with observations of overbank processes and are an improvement over those of previous models which have employed relatively simple representations of floodplain geometry.

KEY WORDS numerical model; floodplain; hydraulics; overbank deposition

INTRODUCTION

Lowland river floodplains are important components of the drainage basin system, acting both as conveyance channels and storage zones during the passage of floodwaves, and as sinks for suspended sediment deposited during such periods of overbank flow. Over the last decade, interest in overbank processes has increased as a result of the need for a better understanding of the suspended sediment dynamics of lowland river systems, increased concern for environmental issues such as the transport and fate of sediment-associated contaminants, and the desire to make predictions regarding the economic impact of flooding. Research into out-of-channel environments has involved two main approaches: first, field-based investigations of the hydraulics of overbank flows (Lewin and Hughes, 1980) and of rates and patterns of floodplain sedimentation (Walling *et al.*, 1986, 1992), and second, the use of numerical and physical models to examine floodplain hydraulics (Krishnappan, 1984) and suspended sediment transport and deposition processes (James, 1985). Flume studies have identified the dominant features of flow hydraulics in compound channels with both straight and meandering geometries (Sellin, 1964; Kiely, 1990), with attention focusing on mass and momentum

* Current address: Department of Geography, University of Exeter, Exeter, Devon, EX4 4RJ, UK.

CCC 0197-9337/97/010059–19

exchange between floodplain and channel elements. Numerical models have also been developed which predict hydraulic variables across a compound channel cross-section for the simplified case of steady longitudinally uniform flow (Shiono and Knight, 1991). Recently, finite difference and finite element schemes have been employed to generate predictions of depth-averaged hydraulic variables in two lateral dimensions (Wijbenga, 1985; Anderson and Bates, 1994). However, despite the considerable potential offered by such approaches, a number of problems remain to be overcome, largely associated with the representation of floodplain topography by such models (Bates *et al.*, 1992). In addition, hydraulic schemes such as these have yet to be coupled with appropriate sediment transport relations, so that physically based models of overbank deposition have been restricted to one- and two-dimensional cross-section oriented approaches (James, 1985; Pizzuto, 1987).

Existing physical and numerical models have successfully replicated many of the processes operating in overbank environments. However, they have as of yet been relatively unsuccessful in terms of replicating the high degree of spatial variability of both hydraulic conditions and sedimentation patterns identified in the field. This paper outlines a numerical model for the prediction of floodplain inundation sequences, overbank deposition rates and deposit grain size distributions which incorporates two main components. The first of these is a simplified hydraulic scheme which predicts flow depths and velocities within a finite difference grid. The second component employs the results of the hydraulic calculations, together with a mass balance relation, to determine patterns of suspended sediment dispersion and deposition over this grid for a range of particle sizes. During the development of this model, emphasis has been placed upon retaining the complicated geometry of natural floodplains, at some expense to the representation of process complexity. The decision to adopt this approach was based upon the belief that this topographic complexity exerts a dominant control on both inundation sequences and patterns of overbank deposition on natural floodplains.

MODEL DEVELOPMENT

Past models of floodplain hydraulics have employed the two-dimensional depth-averaged form of the Navier–Stokes equations (Gee *et al.*, 1990). However, as identified above, obtaining a stable solution to these equations is not always possible in complex topographic environments (Bates *et al.*, 1992). Alternatively, overbank flow patterns have been predicted using the diffusion wave form of the one-dimensional Saint-Venant momentum equation (Cunge *et al.*, 1980). Such an approach offers considerable potential where floodplain geometry is complicated, hence equations of this type have been employed in this study. Despite the relative simplicity of the one-dimensional Saint-Venant momentum equation, compared to the equivalent Navier–Stokes equation, solving equations of this type when utilizing a finite difference grid containing a large number of nodes and representing complex topographic environments remains a time consuming computational procedure. In order to reduce the run-time of the hydraulic component of the numerical model and increase the computer power available for the sediment transport element of the model, a simplified hydraulic approach was adopted here. Rather than solving the equations of fluid motion for the given upstream boundary conditions during each time step of each flood event, these equations were solved initially for a number of upstream water levels in order to generate a set of flow surfaces. These were then used, in conjunction with a relationship between the water levels at the upstream and downstream boundaries of the finite difference grid, to predict hydraulic patterns during all subsequent simulations. The implementation of this approach relies upon the validity of a number of assumptions. First, it is assumed that flood hydrographs can be divided into a number of discrete time intervals, during each of which the discharge crossing the upstream boundary of the solution grid is equal to that crossing the downstream boundary, and that single valued relationships exist between stage and discharge at these boundaries. Second, it is assumed that the patterns of overbank flow experienced within the reach represented by the solution grid do not vary greatly with small changes in upstream water level. Instead they are assumed to be the product of the dominant topographic structures within the reach, so that they vary gradually with increasing stage. This allows hydraulic patterns to be determined for a wide range of flood levels using only a comparatively small number of flow surfaces. Finally, and relating to the first assumption, it is assumed that the patterns of overbank flow within the reach, resulting from a given upstream water level, are similar for separate flood events and for conditions of both rising and falling stage. These assumptions are necessary to simplify the

hydraulic relationships employed in the model. However, it should be noted that in reality overbank flows are characterized by temporal variations (both inter- and intra-flood) and spatial variations in relationships between stage and discharge.

In order to determine the relationship between the water levels at the upstream and downstream boundaries of the finite difference grid representing the study reach, a simple discharge calculation procedure is employed. This involves determining the discharge entering the reach, for a given upstream stage, and calculating the downstream stage required to yield the same discharge leaving the reach. Boundary cross-sections are divided into a number of elements of equal width and discharge components acting normal to these sections are determined for each element from the following equations:

$$h_i = w_b + Sy(y_b - y_i) - z_i \tag{1}$$

$$q_i = \frac{h_i^{5/3} Sx^{1/2}}{n} \Delta y \tag{2}$$

where h_i is the depth of flow over element i, z_i is the bed elevation, n is the Manning roughness coefficient, w_b is the water level at the boundary reference element (i.e. the element for which the boundary water level is specified), y_b and y_i are lateral distances, q_i is the discharge component normal to the boundary of the finite difference grid, Δy is the width of each element, and Sx and Sy are the components of the downstream friction slope in the x and y directions of the finite difference grid (the friction slope is assumed to be equal to the water surface slope). The total discharge crossing the reach boundary in the x direction of the finite difference grid is given by the sum of the discharge components for each element across the relevant section. In Equation 1 it is assumed that floodplain flow moves in a direction parallel to the longitudinal axis of the valley floor and that the elevation of the water surface is constant along lines running perpendicular to this axis. This enables lateral variations in water levels and hence flow depths to be determined where the y axis of the finite difference grid is not parallel to the cross-stream direction of the valley. As with certain other methods for estimating the relationship between stage and discharge (cf. Ervine and Ellis, 1987), Equations 1 and 2 take no account of the impact of momentum transfer between adjacent elements of different depth and velocity, hence they are likely to overestimate the total discharge crossing the boundaries of the model grid (Wormleaton *et al.*, 1982). In addition, the total discharge for a given reference boundary water level (w_b) is strongly dependent upon the values of roughness coefficients and friction slopes employed. In this study, friction slopes were approximated using surveyed floodplain and channel bed slopes at the two boundary cross-sections. Although this method will result in discrepancies between predicted discharges and discharges experienced in the field, it is reasonable to assume that the errors involved will be similar at both upstream and downstream reach boundaries. Furthermore, as it is only the boundary water levels that are carried forward to the next stage of the model, the errors in estimated discharges associated with the technique outlined above have no further impact upon the hydraulic calculations. Optimum floodplain and channel roughness coefficients are determined by calibrating the relationship between upstream and downstream water levels using field measurements of river stage.

The next step in the modelling procedure is to generate the flow surfaces needed to make hydraulic predictions for any given upstream stage. These flow surfaces are termed Water Surface Functions because they describe the water surface elevation at each node in the finite difference grid as a function of the specified upstream water level and the corresponding downstream water level determined using the discharge calculation technique. Water Surface Functions are generated for a number of upstream boundary water levels at 5 cm increments by solving the following continuity of mass and momentum equations:

Continuity of momentum:

$$u = \frac{h^{2/3} Sx^{1/2}}{n} \quad \text{where} \quad Sx = \frac{\partial h}{\partial x} + \frac{\partial z}{\partial x} \tag{3}$$

$$v = \frac{h^{2/3} Sy^{1/2}}{n} \quad \text{where} \quad Sy = \frac{\partial h}{\partial h} + \frac{\partial z}{\partial y} \tag{4}$$

Continuity of mass:

$$\frac{\partial(uh)}{\partial x}+\frac{\partial(vh)}{\partial y}=0 \tag{5}$$

where h is the depth of flow, z is the bed elevation, n is the Manning roughness coefficient and u, v, Sx and Sy are respectively the velocity components and friction slopes in the x and y directions. Equations 3 and 4 are a pair of one-dimensional relationships equivalent to the diffusion wave form of the Saint-Venant momentum equation. The derivation of Equations 3 to 5 involves the neglect of both temporal derivatives and convective acceleration terms, so that friction slopes are approximated by water surface slopes.

The differential Equations 3 to 5 are transformed to a set of difference approximations which are then solved to yield the depth of flow at each node in the finite difference grid for the given upstream and downstream boundary water levels. When a stable approximate solution is obtained the value of the Water Surface Function (f_i) at each wet node is calculated as:

$$f_i=\frac{w_u-h_i-z_i}{w_u-w_d} \tag{6}$$

where w_u and w_d are the specified upstream water level and the corresponding downstream water level determined using the discharge calculation procedure.

Each calculated Water Surface Function is used to predict flow depths and velocities throughout the grid over a specified interval of upstream water levels. This is achieved by rearranging Equation 6 and inserting the relevant boundary water levels, bed elevation and Water Surface Function value. The patterns of flow depth generated in this way are then adjusted in certain places using a simple ponding algorithm, details of which are given in Nicholas (1994). This is necessary because certain floodplain regions containing flowing water at the upstream boundary water level for which the Water Surface Function in use was generated, may be dry or contain ponded water at the slightly lower (i.e. 0–5 cm) upstream water level for which the hydraulic calculations are being made. Two types of ponding are identified by the model: first, backwater ponding where a region is supplied with water from a point downstream, and second, recession ponding where floodplain depressions retain ponded water as the floodplain is drained on the falling limb of the flood hydrograph. Having determined the depth of flow at each node for the given upstream boundary water level, velocity components are calculated in the x and y directions using Equations 3 and 4.

Hydraulic predictions are carried forward to the sediment transport component of the model which predicts patterns of suspended sediment dispersion and deposition for a range of sediment size fractions. This element of the model requires data quantifying the total suspended sediment concentration in the main channel flow and the particle size distribution of this sediment. The depth-integrated mass balance equation for suspended sediment transport by convective and diffusive processes in two horizontal dimensions is then solved for each of these size fractions to allow the sediment concentration and amount of deposition of each fraction to be determined at each floodplain node within the solution grid:

$$(uh)\frac{\partial c}{\partial x}-\frac{\partial}{\partial x}\left(\varepsilon h\frac{\partial c}{\partial x}\right)+(vh)\frac{\partial c}{\partial y}-\frac{\partial}{\partial y}\left(\varepsilon h\frac{\partial c}{\partial y}\right)+D_R=0 \tag{7}$$

where c is the depth-averaged suspended sediment concentration, ε is a horizontal mixing coefficient and D_R is the net rate of deposition (i.e. deposition less erosion and/or resuspension). Horizontal mixing coefficients are determined using standard relationships (cf. Pizzuto, 1987).

$$\varepsilon=\lambda h U_* \tag{8}$$

where λ is a constant which was assigned a value of 0·13 after Fischer *et al.* (1979) and U_* is the shear velocity given by:

$$U_*=(ghSf)^{1/2} \tag{9}$$

where g is the acceleration due to gravity and Sf is the water friction slope (assumed to be equal to the water surface slope). During the development of the model a number of equations predicting net deposition rates

were tested (e.g. Engelund, 1970; Parker, 1978). However, due to the difficulty of applying such equations in situations where flow depths approach zero, we employ a simplified deposition term:

$$D_R = kcVs \tag{10}$$

where Vs is the sediment particle fall velocity and k is an empirical coefficient which controls the proportion of the sediment in suspension at a node that is deposited. This empirical parameter is used to calibrate the model with the aid of measured deposition amounts.

In order to obtain an approximate solution to Equation 7 the terms of this differential equation are written as a series of difference approximations. At the boundary between wet and dry nodes sediment fluxes are set equal to zero to ensure continuity of mass in these regions. When a stable approximate solution to Equation 7 is obtained, the total amount of deposition at each floodplain node during the given time step is determined from:

$$D_i^t = k\Delta t \sum_{j=1}^{J} (Vs_j c_{i,j}^t) \tag{11}$$

where D_i^t is the amount of deposition at node i during the time step t, Δt is the duration of the time step, Vs_j is the fall velocity of the jth size fraction, $c_{i,j}^t$ is the sediment concentration of the jth size fraction at node i during time step t and J is the number of size fractions employed in the model. For most floodplain nodes this represents the total amount of deposition. However, for nodes in areas of the floodplain that are susceptible to recession ponding, there is the additional possibility of this deposition being supplemented by material which settles out in trapped stationary water. The extra sediment contributed in this way is given by:

$$Da_i^t = hp_i \sum_{j=1}^{J} c_{i,j}^{t-1} \tag{12}$$

where Da_i^t is the additional deposition at node i resulting from the settling of trapped sediment, hp_i is the depth of ponded water and $c_{i,j}^{t-1}$ is the sediment concentration of the jth size fraction at node i during the time step prior to the isolation of the ponded area from the main flow. Equation 12 assumes that 100 per cent of the sediment trapped in the ponded water is deposited. The validity of this assumption is dependent upon the time interval between flood events and the significance of flocculation processes within the ponded water.

STUDY AREA AND DATA COLLECTION

Field data needed for model calibration and testing purposes were collected from a 600 m study reach of the River Culm at Rewe in southeast Devon. The River Culm has a drainage area of 276 km^2 above Stoke Canon where it enters the River Exe approximately 5 km north of Exeter. Its lower reaches (Figure 1) are characterized by a meandering gravel-bed channel approximately 12 m wide with fine-grained alluvial banks up to 1·5 m high. The floodplain here is relatively undisturbed (land use is predominantly rough pasture) and substantial inundation occurs on average seven times each year (Lambert and Walling, 1987).

The study reach (Figure 2) has an upstream boundary marked by the river monitoring site at Rewe. A second monitoring station was installed at the downstream reach boundary. The western edge of the reach is delimited by a steep hillslope which provides an excellent vantage point for observing floodwater inundation patterns. To the east, elevation increases more slowly up to the arable land above the valley floor. The 36 ha reach contains a wide variety of topographic features typical of lowland river floodplains. These include depressions, levees, bank breaches, abandoned channels, major and minor drainage ditches, and both straight and meandering channel sections.

The study reach was surveyed in detail using a Geodometer 400 integrated theodolite and EDM unit. Over 3000 points were surveyed on the floodplain surface with the sampling density varying according to topographic complexity. Channel cross-sections were also surveyed at downstream intervals of 10 m along the reach. Interpolation of these data enabled the construction of a finite difference grid with a nodal spacing

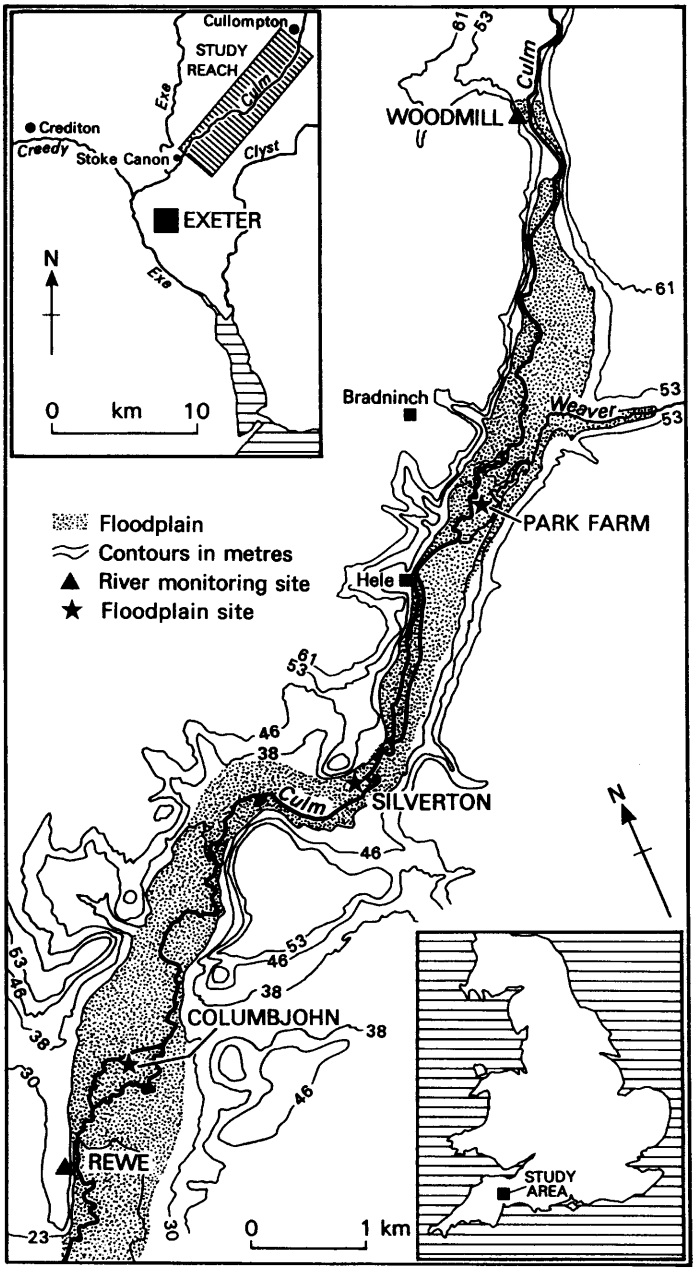

Figure 1. The lower reaches of the River Culm

of 5 m. This scale of resolution allowed complicated topographic features to be represented by the grid with only minimal loss of detail. Figure 3 shows a simplified version of the grid, with a nodal spacing of 10 m for ease of viewing.

River stage and suspended sediment concentration were recorded continuously at the upstream and downstream boundary monitoring sites over a 16 month period from January 1992 to April 1993. Upstream stage measurements provided the input data required by the model, while downstream stage records were

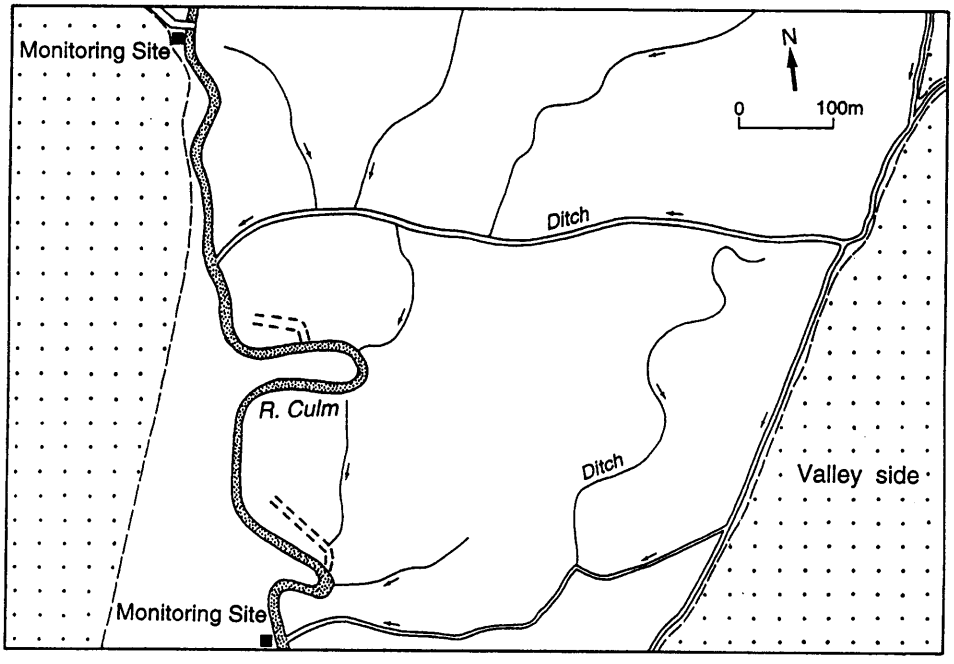

Figure 2. The study reach

employed in the calibration of the discharge calculation procedure. These data were supplemented by information quantifying the particle size distribution and settling characteristics of the transported sediment. In the past, fluvial suspended sediment has generally been characterized by its *ultimate* grain size distribution (i.e. the size distribution of the discrete primary particles of which the load is composed). However, a number of workers (e.g. Ongley *et al.*, 1981; Walling and Kane, 1984; Walling and Woodward, 1993) have highlighted the importance of aggregation in controlling the *in situ* physical properties of suspended sediment. They have shown that the ultimate size distribution of suspended sediment may differ significantly from its *effective* size distribution, which includes composite particles composed of both mineral and organic matter. The settling velocities of composite particles may differ substantially from those of the individual constituent grains. The effective size distribution of the suspended sediment load was measured on ten occasions over the study period using a custom-built water elutriation system. The principles of this system have been both documented and validated by several workers (Beavers and Jones, 1966; Umlauf and Bierl, 1987). The apparatus consists of a series of glass sedimentation chambers through which water is drawn during storm periods. Variations in flow velocities between each chamber, controlled by differences in their cross-sectional areas, cause each to retain sediment particles with a different settling velocity or equivalent spherical diameter. Further details of the system used are given by Walling and Woodward (1993). Using data derived from the elutriation apparatus, the mean contribution to the total load of each of five effective size classes was determined to be: $<8\,\mu$m, 53 per cent; 8–16 μm, 25 per cent; 16–32 μm, 13 per cent; 32–63 μm, 7 per cent and $>63\,\mu$m, 2 per cent. These average values were employed in all model calculations. Because deposition rates are strongly controlled by particle fall velocity, the small amount of material in the coarsest size class makes a disproportionately large contribution to overbank deposits. As a result, this size class was subdivided into two classes with different fall velocities: $>63^{A}\,\mu$m, 1·9 per cent and $>63^{B}\,\mu$m, 0·1 per cent. The latter class represents the very small proportion of large aggregates and coarse sand grains present in the load, which may exceed several hundred micrometres in diameter (Walling and Woodward, 1992).

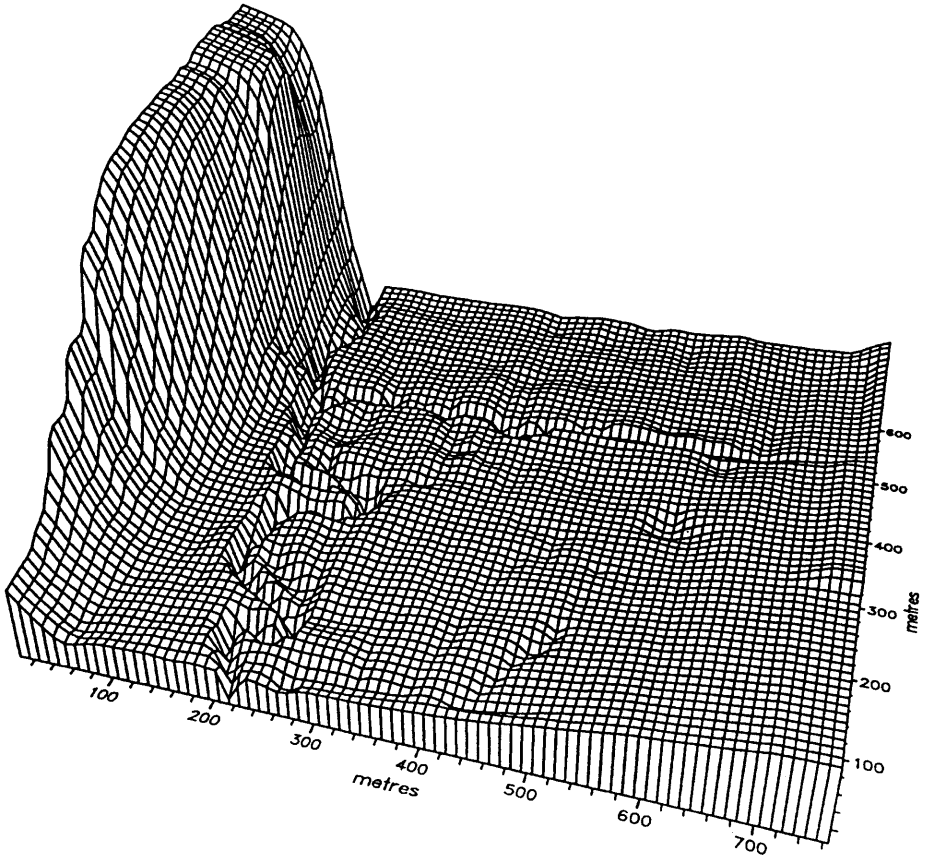

Figure 3. The model's finite difference grid. Nodal spacing is 10 m by 10 m. Vertical exaggeration is 1 : 25

MODEL OPERATION AND RESULTS

The continuous records of boundary water level and suspended sediment concentration were divided into time steps of one hour duration. For each time step the monitored upstream water level and corresponding downstream water level determined using the discharge calculation procedure were used, in conjunction with the relevant Water Surface Function, to determine patterns of flow depth and velocity throughout the finite difference grid. These hydraulic predictions were then used in the sediment transport model component, together with the monitored suspended sediment concentration at the upstream boundary, to determine patterns of suspended sediment dispersion and deposition for each of the grain size fractions employed in the model. Sediment concentrations monitored at the downstream boundary were compared with those at the upstream boundary to validate the assumption that this variable is approximately constant within the main channel during a given time step.

Figure 4 presents a record of the upstream boundary data, together with both the monitored and predicted downstream water levels, for the flood event of 30 November to 5 December 1992. All stage data are given relative to the mean elevation of the channel bed at the downstream reach boundary. The data in Figure 4 give some indication of the accuracy of the predictions of the water level at the downstream reach boundary. The mean absolute error between predicted and observed water levels at this point is approximately 3 cm for this flood event. In general, there is a tendency for the model to underpredict downstream stage when the observed stage lies between approximately 1·35 m and 1·55 m. Outside these limits the model tends to overpredict the downstream stage. Because the relationship between stage and discharge in the field exhibits

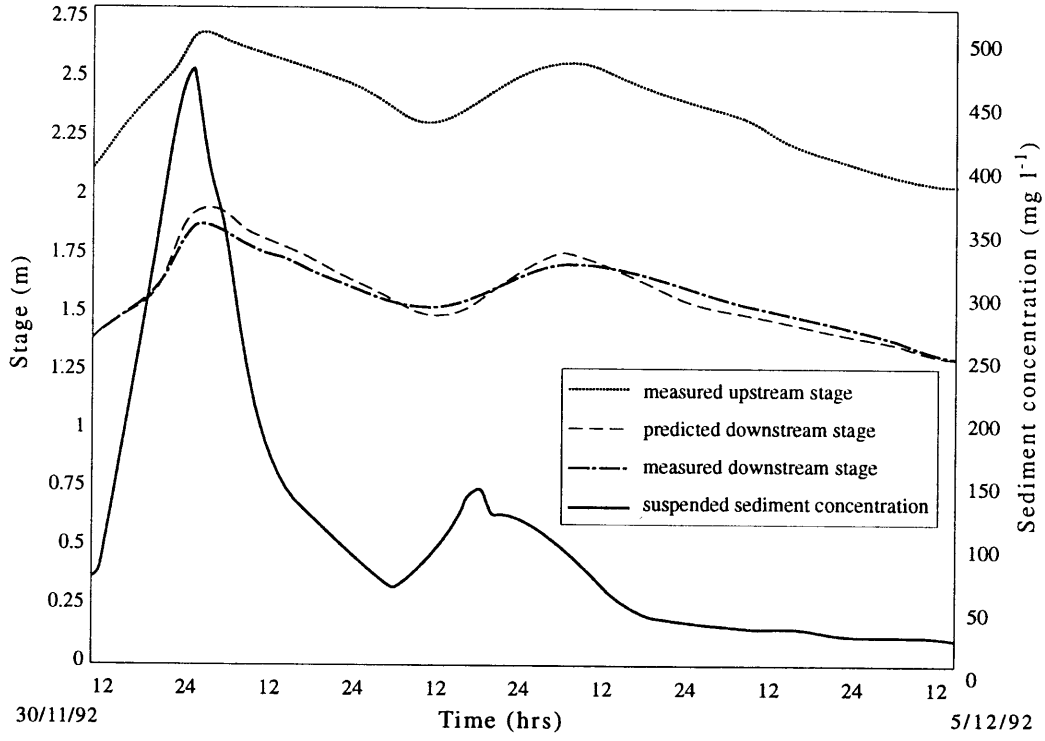

Figure 4. Monitored suspended sediment concentration (mg l^{-1}), monitored upstream and downstream stage (m) and predicted downstream stage (m) for the flood event of 30 November to 5 December 1992

hysteresis, temporal variations in the accuracy of model predictions occur. In particular, observed downstream water levels are slightly higher on the falling limb of floods than on the rising limb, hence they are more likely to be overpredicted on the latter than on the former.

Figure 5 shows the predicted pattern of flow depth within the study reach for an upstream water level of 2·35 m. In addition to providing a snapshot of the complicated inundation patterns predicted by the model at this intermediate stage of flooding, Figure 5 can also be used to illustrate the complex sequence of floodplain inundation. The average width of the water surface in this figure is approximately 400 m; however, overbank flow is in fact concentrated in a number of narrower low-lying drainage ditches and depressions. Furthermore, several emergent floodplain areas exist, the most notable of which is the well developed levee marking the eastern side of the channel in the upstream portion of the study reach (A). Flow depths of greater than 0·5 m are common in the drainage ditches and in the abandoned channel segment which border the floodplain in the downstream half of the reach (B). These are amongst the first areas to be inundated, along with low-lying upstream regions (C and D), as a result of backwater ponding from the main channel. As flood levels rise, ponded water extends into other areas (E and F), and shallow floodplain drainage ditches begin to convey flow (G), even prior to their connection with main channel bank breaches (H). By the time flood levels reach those shown in Figure 5, many of these discrete inundation zones have become interconnected. As stage rises further, emergent floodplain areas shrink and floodplain water begins to flow less as a collection of separate flow streams and more as a single unit in the general direction of the valley bed slope.

Because of the difficulty of obtaining detailed measurements of hydraulic variables at the spatial and temporal scales under examination, an attempt was made to assess the accuracy of model predictions by using a series of ground photographs of floodwater extent, supplemented by observations of floodwater inundation mechanisms. Observed inundation patterns for the flood shown in Figure 4 closely followed

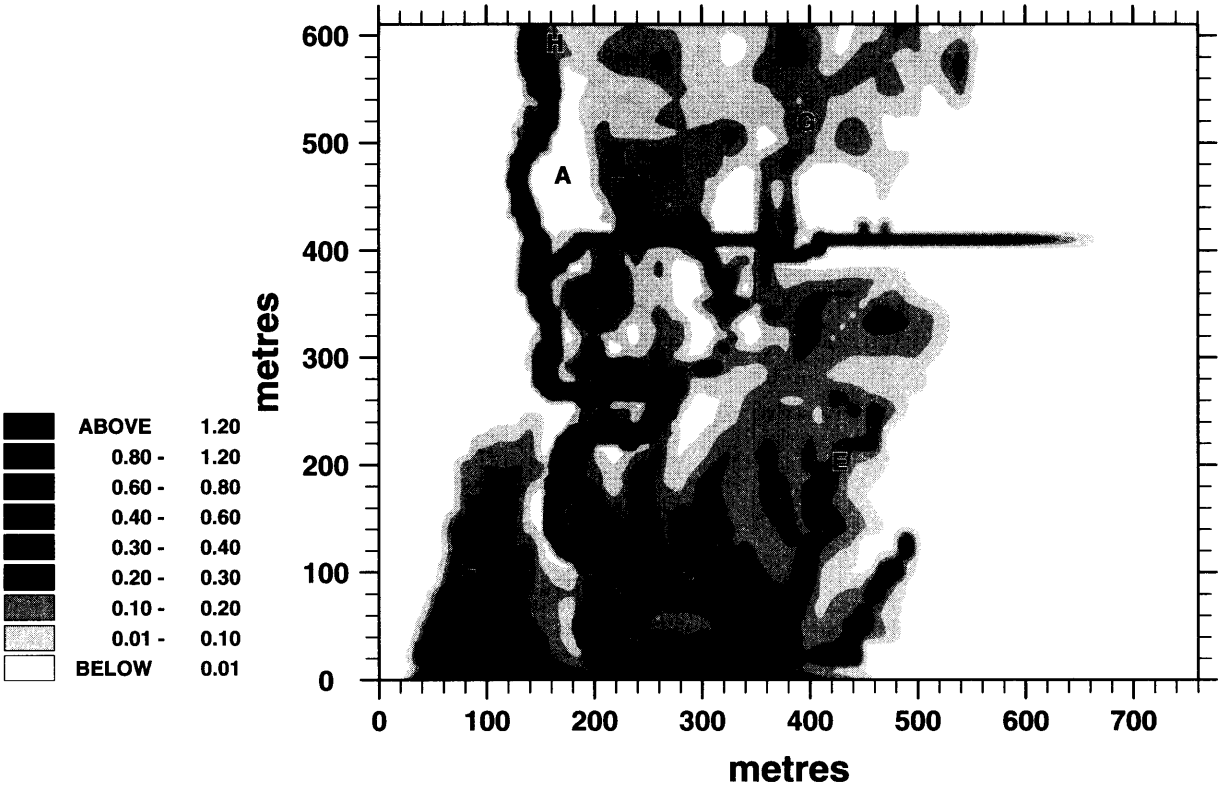

Figure 5. Predicted pattern of flow depth within the study reach for an upstream water level of 2·35 m

the sequence of events outlined briefly above. In particular, the model predicts accurately the positions where bank breaching and backwater ponding occurred in the field. Despite this, the predicted water levels at which observed inundation thresholds were exceeded are typically in error by 0–5 cm. Furthermore, at downstream boundary water levels above approximately 1·6 m the model overpredicts inundation extends in the downstream portion of the reach. This probably reflects the overprediction of the downstream boundary water level by the discharge calculation procedure.

Figure 6 shows the predicted pattern of total suspended sediment concentration (as a percentage of that in the main channel) for the main peak of the flood shown in Figure 4. Predicted suspended sediment concentrations decrease away from the main channel at highly spatially variable rates that are controlled by local flow conditions. Peak suspended sediment concentrations occur throughout the channel belt in the downstream half of the study reach. This region is occupied by deep flows moving at velocities of up to $0{\cdot}5\,m\,s^{-1}$ in directions perpendicular to the channel in the meander bends. As a result, the longitudinal convective term in Equation 7 dominates the mass balance relation at floodplain nodes within the channel belt, and suspended sediment concentrations are therefore high throughout this zone. Outside the channel belt, floodplain convective currents move in directions approximately parallel to the main channel, and suspended sediment concentrations decline away from the latter at rates controlled by local topography and thus hydraulics. In general, both flow velocities and mixing coefficients increase in proportion to flow depths and water surface slopes. Hence, where bank breaches occur and where drainage ditches lead away from the main channel, rates of suspended sediment dispersion are greater than in the lee of barriers to the flow such as levees.

As indicated above, the deposition term employed in the sediment transport component of the model

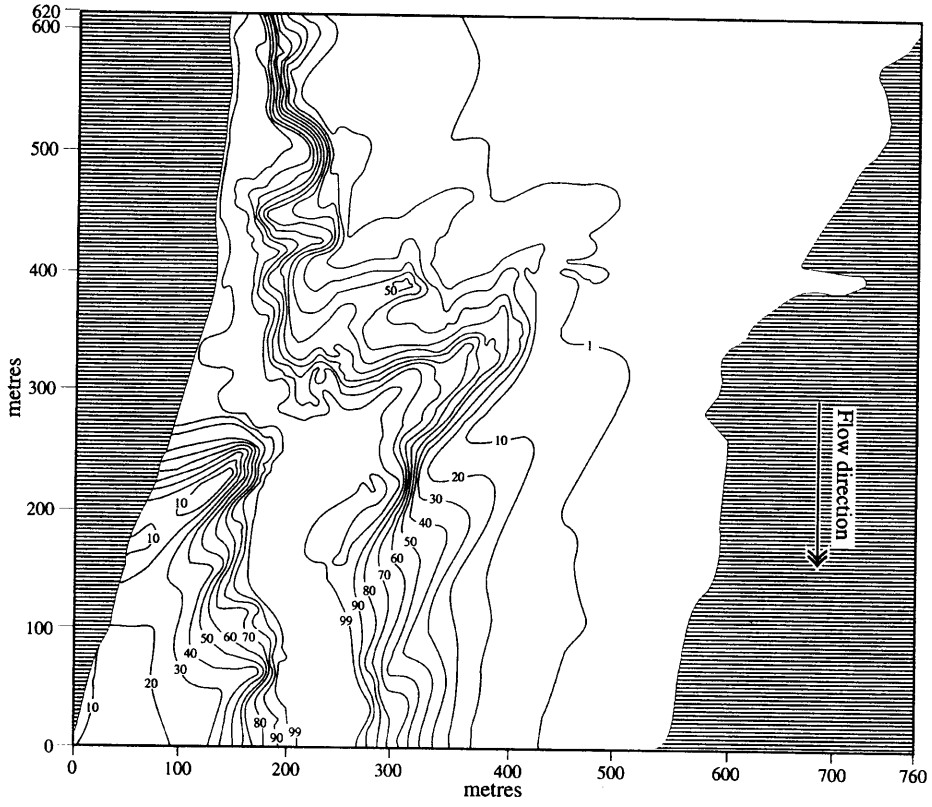

Figure 6. Predicted pattern of suspended sediment concentration (as a percentage of that in the main channel) for the peak of the flood event of 30 November to 5 December 1992

contains an empirical coefficient (k) which was used to calibrate the model. This was achieved with the aid of direct measurements of overbank deposition, which were obtained for nine flood events during the 16 month study period using Astroturf sedimentation traps (cf. Lambert and Walling, 1987). These consisted of 1·5 cm tufts of artificial grass attached to a pliable base and fixed to the floodplain surface using six inch steel pins. Traps were deployed in closely spaced groups of nine to give an indication of the degree of measurement variability involved in their utilization. Trap locations were surveyed and fixed upon the model's finite difference grid to allow direct comparison between measured and predicted deposition amounts. Traps were installed during times of low flow and retrieved from the floodplain following the subsidence of floodwaters. In total, 52 sets of sedimentation traps were employed during the study period. Predictions of deposition amounts for each trap set were compared with measured deposition amounts, and the value of the parameter (k) was adjusted manually so as to reduce the total error for the dataset as a whole. Using this procedure k was assigned a value of 1/30. Varying the value of k adjusts deposition amounts over the whole floodplain by a factor which (across the range of realistic k values) shows only very small local variations. As a result, the calibration procedure has a negligible effect upon predicted spatial and temporal variations in relative deposition amounts.

Figure 7 shows a scatter plot of predicted versus measured deposition amounts (the line of perfect agreement between the two is also shown). The mean absolute error for the 52 data points is 130 g m^{-2} while the mean percentage error is 61 per cent. Although the latter figure may appear high, it should be noted that a large proportion of this error is associated with a small number of data points for which absolute errors are in fact low. Figures 8a and 8b show scatter plots of the ratio of measured to predicted deposition amounts

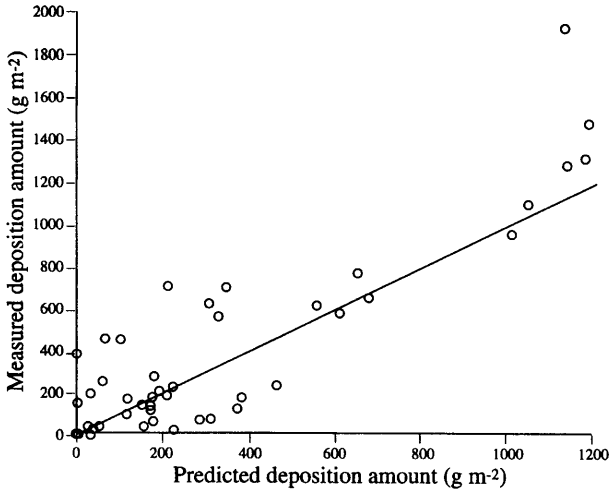

Figure 7. Measured and predicted deposition amounts ($g\,m^{-2}$) for the dataset of 52 points derived using Astroturf sedimentation traps

versus distance from the main channel and relative elevation respectively (the latter variable represents an adjustment of the actual elevation to compensate for down-valley reductions in mean elevation). Figure 8a suggests a weak trend towards increasing underprediction of deposition amounts away from the main channel. No clear trend is apparent in Figure 8b, but the maximum and minimum values of the ratio of measured to predicted deposition amounts become respectively higher and lower as relative elevation increases, thus implying that model predictions become generally less accurate in elevated floodplain regions.

Figure 9 shows the predicted pattern of overbank deposition amounts within the study reach for the flood event of 30 November to 5 December 1992. Calibration of the model using the mat dataset controls the absolute deposition amounts predicted by the model; however, it has little or no influence on relative spatial patterns predicted by the model. Predicted amounts of deposition for this flood are highest in the low-lying areas close to the main channel. These include the two abandoned channel segments, the entrances to several minor floodplain drainage ditches, low points in the levees that run along the channel and the downstream margins of the floodplain inside the meander bends. The general pattern of decreasing deposition with distance from the channel can be attributed not only to a decrease in suspended sediment concentrations away from the source of sediment, but also to increasing floodplain elevation and reduced durations of inundation. The extensive areas where deposition amounts exceed $300\,g\,m^{-2}$ in the downstream portion of the reach reflect the lower relative elevations and increased channel sinuosity in these regions. These factors promote high suspended sediment concentrations and increased deposition rates within the channel belt. The well developed levee in the upstream half of the reach reduces deposition amounts by restricting the supply of water and sediment to the floodplain in its lee. Although prior to the overtopping of the levee these areas are inundated by ponded water from the major drainage ditch and by water supplied by the shallow drainage pathways which dissect the upstream reach boundary, the low concentrations of suspended sediment which characterize these sources result in deposition amounts which are an order of magnitude lower than those in many downstream areas.

The model predictions presented in Figures 7, 8 and 9 compare favourably with those of previous models of overbank deposition (e.g. James, 1985; Pizzuto, 1987) in that they indicate increasing deposition amounts close to the main channel and in low-lying areas. Despite this, given the limited nature of the mat dataset and the fact that these data have already been employed in model calibration, it is difficult to assess the relationship between spatial patterns of predicted and measured deposition amounts. A more rigorous assessment of model accuracy would demand the use of an extensive independent dataset. Such an examination, based

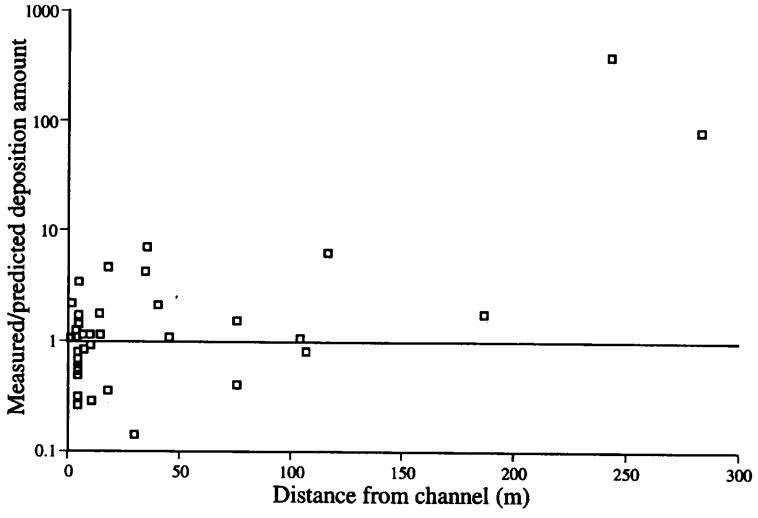

(a)

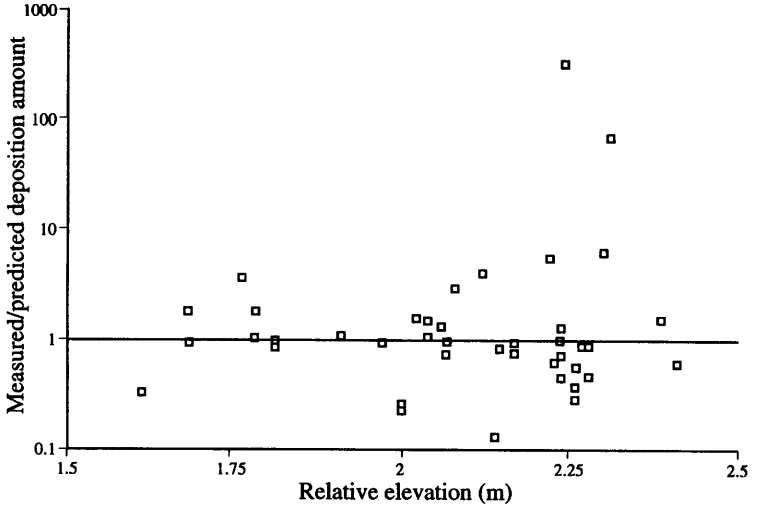

(b)

Figure 8. The ratio of the measured to predicted deposition amounts plotted against (a) the distance from the main channel of the sampling points, and (b) the relative elevation of the sampling points

upon detailed maps of medium-term overbank deposition rates (30–40 years), generated using ^{137}Cs measurements, will be presented elsewhere (Nicholas and Walling, in press). However, in order to provide some independent evidence of the model's success at predicting spatial patterns of deposition, a brief summary of some of these results is presented here.

Caesium-137 is an artificial fallout radionuclide associated with the testing of nuclear weapons during the period from the mid 1950s to the mid-1960s. Additional releases of ^{137}Cs have subsequently occurred, including that resulting from the Chernobyl accident in 1986. Following deposition as fallout, radiocaesium is strongly adsorbed by clay particles in the surface horizons of the soil (Frissel and Pennders, 1983; Livens and Rimmer, 1988), and its subsequent redistribution in the landscape, in association with sediment particles, may be used to determine rates and patterns of sediment movement (Ritchie and McHenry, 1990; Walling and Bradley, 1990).

In this study the ^{137}Cs whole core approach to documenting rates of floodplain deposition, as described by

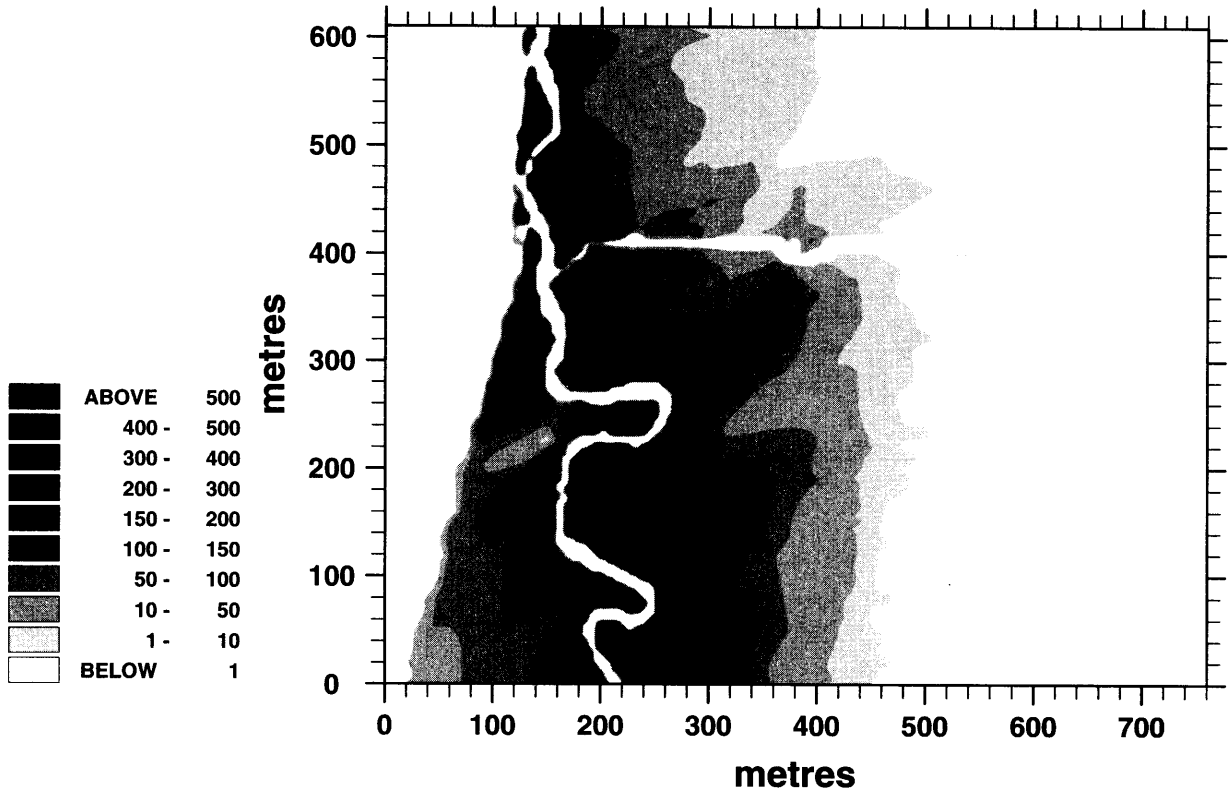

Figure 9. Predicted pattern of total deposition amounts ($g\,m^{-2}$) for the flood event of 30 November to 5 December 1992

Walling and Bradley 1990) and Walling *et al.* (1992), was employed. This involves the determination of total ^{137}Cs inventories ($m\,Bq\,cm^{-2}$) for single whole cores obtained from floodplain sites. These inventories are then compared with a reference inventory representative of the level of caesium activity in a nearby undisturbed soil profile located above the level of the floodplain. Floodplain ^{137}Cs inventories in excess of this reference level indicate net accumulation of sediment and associated radiocaesium. If the mean ^{137}Cs content of the deposited sediment can be estimated, this excess value can be converted to a mean rate of floodplain sedimentation.

Floodplain cores were obtained to depths of 50 cm using a Cobra percussion corer fitted with a steel core tube with an internal diameter of 6·9 cm. The core samples were air dried and disaggregated before the ^{137}Cs content of the <2 mm fraction was determined by gamma spectrometry using a high purity germanium detector equipped with a multi-channel analyser. Counting times were in excess of 25 000 s giving an analytical precision of approximately ± 6 per cent (2 st. dev.).

Owing to the preferential association of ^{137}Cs with the clay fraction of deposits (Walling and Woodward, 1992), the use of a single value for the mean caesium content of deposited material may introduce error in the estimation of sedimentation rates. Accordingly, the mean caesium content of deposited material was estimated separately for each whole core. Estimates of the mean ^{137}Cs content of deposited material were derived from four detailed caesium profiles collected from markedly different locations within the study reach. These data were used, in conjunction with measured grain size distributions for the surface sediment at these four sites, to determine a relationship between sediment particle size and mean caesium content. The mean caesium content of deposited material was then estimated for each whole core by employing the grain size distribution of the floodplain sediment at the given sampling location predicted by the numerical model.

Medium-term model predictions of sedimentation rates were generated by calculating the deposition rate for a given upstream water level and weighting this by the frequency of occurrence of that water level, using flow data provided by the National Rivers Authority (Southwest Division). As a result, model predictions represent mean annual deposition rates based upon mean annual flow conditions and current floodplain topography. In contrast, caesium-based estimates of mean annual deposition rates will have been influenced by the impact on floodwater hydraulics, and hence deposition rates, of increases in floodplain elevation over time. The neglect of this feedback by the model was calculated to result in predictions which were, at worst (i.e. close to the main channel), 10 per cent lower than deposition rates estimated using the caesium data.

A single valued relationship between the water level and the suspended sediment concentration at the upstream reach boundary, for use in the model, was determined from records of these variables measured at the river monitoring station at Rewe over a 16 month period. Considerable scatter exists in the monitored suspended sediment data reflecting inter- and intra-storm variations in catchment sediment production. However, the linear trend fitted to these data is deemed to be a reasonable first approximation for the purpose of determining deposition rates over such an extended period (i.e. 30–40 years).

Figure 10a shows the topography of a floodplain site adjacent to the main channel at which 60 floodplain cores were obtained. The dominant features of this location are two small depressions located 10 m from the main channel. These are inundated by backwater ponding during the early stages of flooding. During floodwater recession, both depressions retain ponded water trapped behind a lip of raised ground separating them from the main channel.

Figures 10b and 10c show respectively the mean annual deposition rates predicted by the numerical model and those estimated using the ^{137}Cs data for this site. Predicted and estimated deposition rates are broadly similar, with peak rates of approximately 6 mm a^{-1} close to the channel and declining deposition rates at greater distances and increased floodplain elevations. The locally increased deposition rates (3 mm a^{-1}) within the two closed depressions, which result from the deposition of fine sediment carried by the ponded water trapped in these features during floodwater recession, are also reproduced by model predictions. However, a number of differences between model predictions and caesium-based estimates can be identified. Apart from differences in contour shape between these two figures, two areas of high estimated deposition rates are not present in the model predictions. The first, close to the apex of the bend, may be attributed to inadequate representation of near-bank floodplain elevations by the model, due to the restrictive nature of the finite difference grid employed. The second, located 25–30 m from the main channel, lies on the valley side at the limit of current inundation extent, hence it may reflect the impact of human interference on floodplain caesium inventories.

The deposition amounts and rates shown in Figures 7 to 10 represent the sum of the contributions from each of the six effective size classes employed in the model. As a result of the breakdown of sediment aggregates following their deposition, it is not possible to measure the effective size distributions of deposited sediment. Hence, previous studies of overbank deposition have described the particle size characteristics of flood deposits in terms of their ultimate size distributions (cf. Marriott, 1992; Simm, 1993). Similarly here, samples of deposited sediment retrieved from the Astroturf sedimentation traps were analysed in the laboratory and their ultimate grain size distributions were determined using a Malvern Mastersizer MS20. Ultimate size distributions were also determined for material in each of the effective size classes employed in the model. This was achieved using samples of suspended sediment obtained from the water elutriation system. Ultimate size distributions for the material in each effective size class were then used, in conjunction with the predicted effective size distributions determined for the trap locations, to calculate predicted ultimate size distributions for comparison with the measured ultimate size distributions determined for the corresponding samples.

Figure 11 shows the predicted effective, predicted ultimate and measured ultimate grain size distributions for three typical flood deposits. The $>63^{A}$ μm and $>63^{B}$ μm effective size fractions have been lumped into one class for these purposes because insufficient sediment was available to determine an ultimate size distribution separately for each. The results for each of the three samples clearly illustrate two main features: first, there is a reasonable level of agreement between the measured and predicted ultimate grain size distributions,

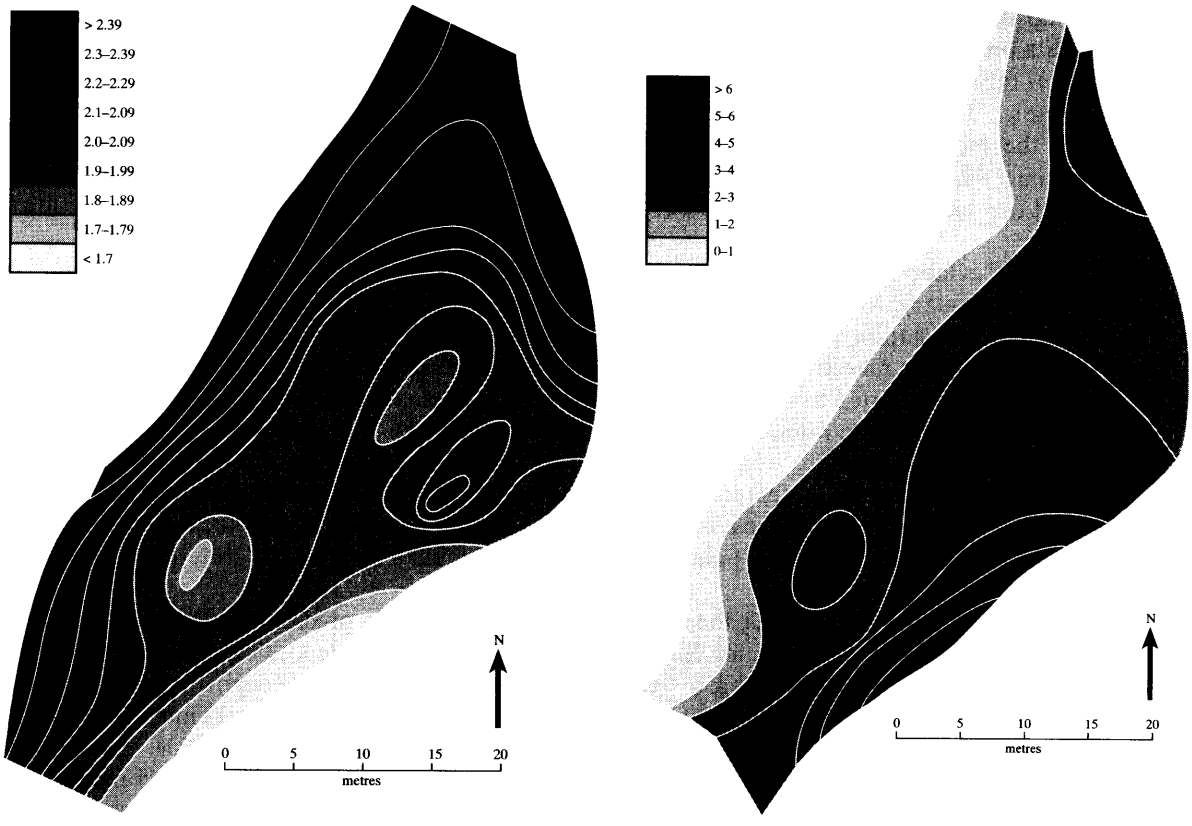

Figure 10. (a) Floodplain elevation (m) relative to an arbitrary datum. (b) Model predictions of mean annual deposition rates (mm a^{-1}). (c) Caesium-based estimates of mean annual deposition rates (mm a^{-1})

and second, there is a sharp contrast between the ultimate and effective grain size distributions. The former tend to be composed of approximately 50 per cent material in the $<8\,\mu$m class, with the remaining 50 per cent spread fairly evenly over the other four size classes. In contrast, the effective size distributions comprise roughly 65 per cent material $>32\,\mu$m in diameter, with decreasing proportions in the smaller size fractions. Clearly, the size distribution of the aggregated sediment deposited on the floodplain is very different to that of the discrete grains comprising these composite particles.

Examining the samples individually gives an indication of spatial variations in the grain size characteristics of deposits. Sample M3 is an example of a near-channel flood deposit. For deposits of this type, the relative contribution of each of the effective size classes increases from fine to coarse. This occurs because close to the main channel the relatively high fall velocities of coarse size fractions outweigh their low relative contribution to the sediment in the water column. Sample M30 represents a deposit characteristic of greater distances from the main channel. Depletion of the $>63\,\mu$m fraction of the load over the region separating this sampling point from the channel has caused the 32–63 μm size class to become the biggest single contributor of sediment to this deposit. Sample M38 was obtained from a location susceptible to the influence of recession ponding. Given sufficient time, all the sediment carried by the water trapped in such a closed depression following the recession of floodwaters is deposited, hence particle fall velocity is no longer an important factor controlling deposition rates. This results in the very high contributions of material in the $<8\,\mu$m size classes for both effective and ultimate size distributions.

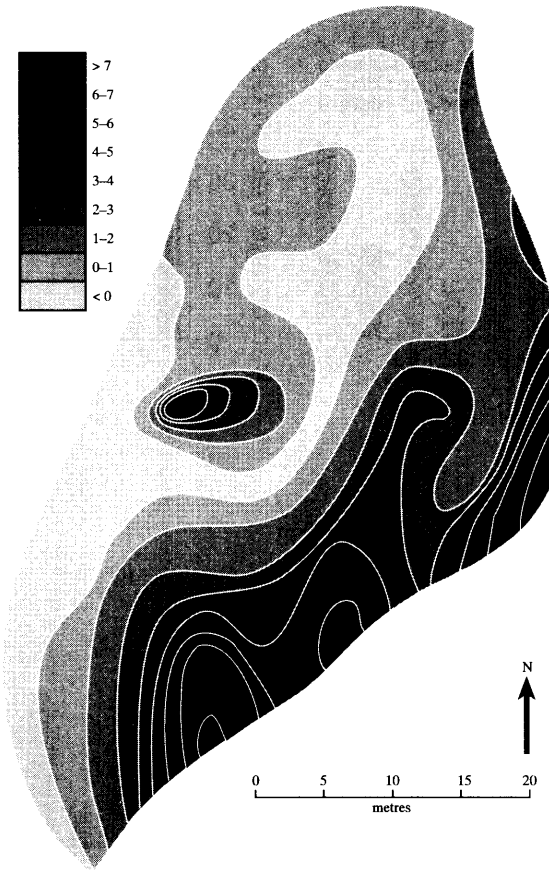

Figure 10 (continued)

CONCLUSIONS

Past models of overbank hydraulics (Gee *et al.*, 1990; Shiono and Knight, 1991) and overbank sedimentation (James, 1985; Pizzuto, 1987) have employed relatively simple representations of floodplain topography. Thus, although they have generated meaningful patterns of floodwater flow depths and velocities and overbank deposition amounts, their predictions have not always been easily related to the more complex spatial and temporal distributions of these variables identified by field workers (cf. Lewin and Hughes, 1980; Walling *et al.*, 1992). In an attempt to address this issue, a numerical model is presented which is based upon simple finite difference approximations of hydraulic and suspended sediment transport relations applied to a finite difference grid which incorporates a realistic representation of natural floodplain geometries. Although this approach necessitates a reduction in the complexity of the process equations employed, it has been shown to enable the accurate simulation of detailed inundation sequences and patterns of suspended sediment dispersion and deposition.

Simulated inundation sequences have been shown to be complicated and controlled by the complex floodplain topography. During the early stages of flooding, inundation patterns are largely a product of backwater ponding effects in drainage ditches and other low-lying areas. As water levels rise, inundated areas become interconnected so that a number of distinct flow regions are created. As stage increases further, the emergent areas between these flow paths shrink and floodwater flow directions are influenced less by local topographic structures and more by the overall geometry of the valley floor.

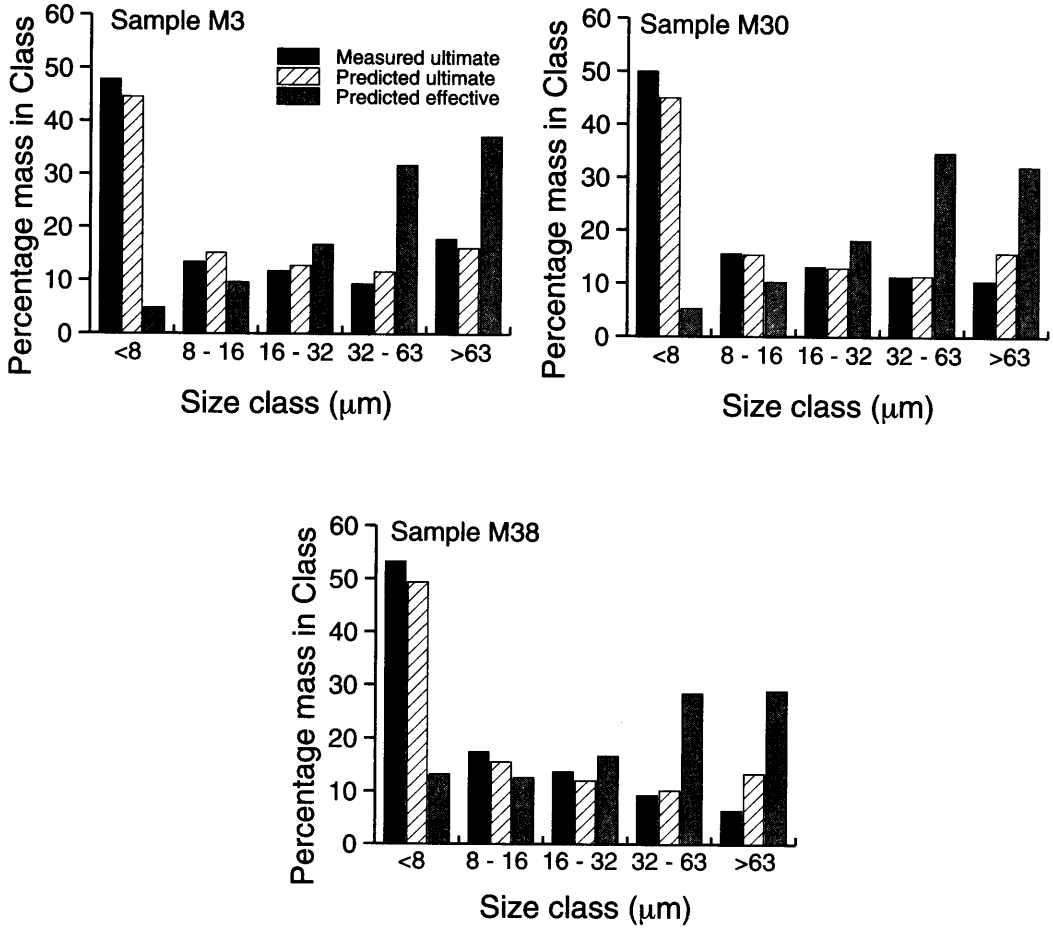

Figure 11. Predicted effective, predicted ultimate and measured ultimate grain size distributions for three representative flood deposits

These hydraulic patterns affect overbank deposition amounts by controlling the frequency of inundation and the magnitude of local suspended sediment concentrations. Within the channel belt, above a critical stage threshold, suspended sediment transport processes are dominated by longitudinal convective currents which promote high concentrations of suspended sediment and high rates of overbank deposition. Outside the channel belt, convective currents acting perpendicular to the channel are weak, and suspended sediment transport is therefore strongly influenced by diffusive mechanisms. In these areas, sediment concentrations, and thus deposition rates, are highly spatially variable. Patterns of these variables are controlled by both local and more distant floodplain topography, which determine the point in the channel from which suspended sediment is supplied and the transport (hydraulic) conditions in the intervening regions.

ACKNOWLEDGEMENTS

The authors gratefully acknowledge the support of the UK Natural Environment Research Council in providing a Postgraduate Studentship for work on overbank sedimentation in Devon rivers. The assistance of the National Rivers Authority in providing hydrologic records and the cooperation of local landowners in permitting access to floodplain sites are also acknowledged with gratitude.

REFERENCES

Anderson, M. G. and Bates, P. D. 1994. 'Evaluating data constrains on two dimensional finite element models of floodplain flow', *Catena*, **21**, 1–15.

Bates, P. D., Anderson, M. G., Baird, L., Walling, D. E. and Simm, D. J. 1992. 'On the potential for using two-dimensional finite element schemes in geomorphological investigations of floodplain environments', *Earth Surface Processes and Landforms*, **17**, 575–588.

Beavers, A. H. and Jones, R. L. 1966. 'Elutriation for fractionating silts', *Soil Science Society of America Proceedings*, **30**, 126–128.

Cunge, J. A., Holly, F. M. and Verwey, A. 1980. *Practical Aspects of Computational River Hydraulics*, Pitman, London, 420 pp.

Engelund, F. 1970. 'Instability of erodible beds', *Journal of Fluid Mechanics*, **42**, 225–244.

Ervine, D. A. and Ellis, J. 1987. 'Experimental and computational aspects of overbank floodplain flow', *Transactions of the Royal Society of Edinburgh: Earth Sciences*, **78**, 315–325.

Fischer, H. B., List, E. J., Koh, R. C. Y., Imberger, J. and Brooks, N. H. 1979. *Mixing in Inland and Coastal Waters*, Academic Press, London, 483 pp.

Frissel, M. J. and Pennders, R. 1983. 'Models for the accumulation and migration of ^{90}Sr, ^{137}Cs, $^{239,240}Pu$, and ^{241}Am in the upper layer of soils', in *Ecological Aspects of Radionuclide Release*, Special Publication of the British Ecological Society, **3**, 63–72.

Gee, D. M., Anderson, M. G. and Baird, L. 1990. 'Large-scale floodplain modelling', *Earth Surface Processes and Landforms*, **15**, 513–523.

James, C.S. 1985. 'Sediment transfer to overbank sections', *Journal of Hydraulic Research*, **23**, 435–452.

Kiely, G. 1990. 'Overbank flow in meandering compound channels: the important mechanisms', in White, W. R. (Ed.), *International Conference on River Flood Hydraulics*, Wiley, Chichester, 207–213.

Krishnappan, B. G. 1984. 'Laboratory verification of turbulent flow model', *Journal of Hydraulic Engineering*, **110**, 500–514.

Lambert, C. P. and Walling, D. E. 1987. 'Floodplain sedimentation: A preliminary investigation of contemporary deposition within the lower reaches of the River Culm, Devon, UK', *Geografiska Annaler*, **69A**, 393–404.

Lewin, J. and Hughes, D. 1980. 'Welsh floodplain studies. II: Application of a qualitative inundation model', *Journal of Hydrology*, **46**, 35–49.

Livens, F. R. and Rimmer, D. L. 1988. 'Physico-chemical controls on artificial radionuclides in soils', *Soil Use and Management*, **4**, 39–63.

Marriott, S. 1992. 'Textural analysis and modelling of a flood deposit: River Severn, UK', *Earth Surface Processes and Landforms*, **17**, 687–697.

Nicholas, A. P. 1994. *Modelling overbank deposition on floodplains: A case study of the River Culm, Devon*, unpublished Ph.D. thesis, University of Exeter.

Nicholas, A. P. and Walling, D. E. 1997. 'Investigating spatial patterns of medium-term overbank sedimentation on floodplains: A combined numerical modelling and radiocaesium-based approach.' *Geomorphology*. In press.

Ongley, E. D., Bynoe, M. C. and Percival, J. B. 1981. 'Physical and geochemical characteristics of suspended solids, Wilton Creek, Ontario', *Canadian Journal of Earth Sciences*, **18**, 1365–1379.

Parker, G. 1978. 'Self-formed straight rivers with equilibrium banks and mobile bed: I-the sand-silt river', *Journal of Fluid Mechanics*, **89**, 109–125.

Pizzuto, J. E. 1987. 'Sediment diffusion during overbank flows', *Sedimentology*, **34**, 301–317.

Ritchie, J. C. and McHenry, J. R. 1990. 'Application of radioactive fallout cesium-137 for measuring soil erosion and sediment accumulation rates and patterns: A review', *Journal of Environmental Quality*, **19**, 215–233.

Sellin, R. H. J. 1964. 'A laboratory investigation into the interaction between flow in the channel of a river and that of its floodplain', *La Houille Blanche*, **7**, 793–801.

Shiono, K. and Knight, D. W. 1991. 'Turbulent open-channel flows with variable depth across the channel', *Journal of Fluid Mechanics*, **222**, 617–646.

Simm, D. J. 1993. *The deposition and storage of suspended sediment in contemporary floodplain systems: A case study of the River Culm, Devon*, unpublished Ph.D. Thesis, University of Exeter.

Umlauf, G. and Bierl, R. 1987. 'Distribution of organic micropollutants in different size fractions of sediment and suspended solid particles of the River Rotmain. *Zeitschrift Wasser-Abwasser Forsch.* **20**, 203–209.

Walling, D. E. and Bradley, S. B. 1990. 'Some applications of caesium-137 measurements in the study of fluvial erosion, transport and deposition', *Erosion, Transport and Deposition Processes*, IAHS Publication No. 189, Wallingford, U.K. 179–203.

Walling, D. E. and Kane, P. 1984. 'Suspended sediment properties and their geomorphological significance', in Burt, T. P. and Walling, D. E. (Eds), *Catchment Experiments in Fluvial Geomorphology*, Geobooks, Norwich, U.K. 311–334.

Walling, D. E. and Woodward, J. C. 1992. 'Use of radiometric fingerprints to derive information on suspended sediment sources', in *Erosion and Transport Monitoring Programmes in River Basins*, IAHS Publication No. 210, Wallingford, U.K. 153–164.

Walling, D. E. and Woodward, J. C. 1993. 'Use of a field-based water elutriation system for monitoring the *in situ* particle size characteristics of fluvial suspended sediment, *Water Research*, **27**, 1413–1421.

Walling, D. E., Bradley, S. B. and Lambert, C. P. 1986. 'Conveyance losses of suspended sediment within a floodplain system', in *Drainage Basin Sediment Delivery*, IAHS Publication No. 159, Wallingford, U.K. 119–131.

Walling, D. E., Quine, T. A. and He, Q. 1992. 'Investigating contemporary rates of floodplain sedimentation', in Carling, P. A. and Petts, G. E. (Eds), *Lowland Floodplain Rivers: Geomorphological Perspectives*, Wiley, Chichester, 165–184.

Wijbenga, J. H. A. 1985. 'Steady depth-averaged flow calculations on curvilinear grids', in *Second International Conference on the Hydraulics of Floods and Flood Control*, Cambridge, 373–387.

Wormleaton, P. R., Allen, J. and Hadjipanos, P. 1982. 'Discharge assessment in compound channel flow', *Journal of the Hydraulics Division*, **108**, 975–994.